Lattice dynamics of bismuth tellurohalides

I. Yu. Sklyadneva,[1,2,3,4] R. Heid,[1] K.-P. Bohnen,[1] V. Chis,[2] V. A. Volodin,[5,6] K. A. Kokh,[7] O. E. Tereshchenko,[5,6] P. M. Echenique,[2,8,9] and E. V. Chulkov[2,8,9]

[1]*Institut für Festkörperphysik, Karlsruher Institut für Technologie, D-76021 Karlsruhe, Germany*
[2]*Donostia International Physics Center, 20018 San Sebastián/Donostia, Basque Country, Spain*
[3]*Tomsk State University, 634050, Tomsk, Russian Federation*
[4]*Institute of Strength Physics and Materials Science, pr. Academicheskii 2/1,634021, Tomsk, Russian Federation*
[5]*Institute of Semiconductor Physics, Novosibirsk, 630090 Russian Federation*
[6]*Novosibirsk State University, Novosibirsk, 636090 Russian Federation*
[7]*Institute of Geology and Mineralogy, SB RAS, Novosibirsk 630090, Russian Federation*
[8]*Departamento de Física de Materiales, Facultad de Ciencias Químicas, Universidad del País Vasco - Euskal Herriko Unibertsitatea, Apdo. 1072, 20080 San Sebastián/Donostia, Basque Country, Spain*
[9]*Centro de Física de Materiales, Materials Physics Center, Centro Mixto, Universidad del País Vasco - Euskal Herriko Unibertsitatea, 20018 San Sebastian/Donostia, Spain*

(Received 3 July 2012; published 4 September 2012)

Lattice dynamics of two bismuth tellurohalides, BiTeI and BiTeCl, and the influence of spin-orbit coupling on their vibrational properties are investigated using first-principles calculations in the density functional perturbation formalism. We also report on the Raman study of these bismuth tellurohalides as well as BiTeBr. It is shown that the inclusion of spin-orbit interaction results in a sizable softening of the phonon spectra of BiTeI and BiTeCl. For both compounds a strong anisotropy in the dielectric tensor and in the Born effective charges is found. Predicted Raman active mode frequencies in BiTeI and BiTeCl are in good agreement with the experimental Raman data.

DOI: 10.1103/PhysRevB.86.094302 PACS number(s): 63.20.D−, 63.20.dk, 78.30.−j

I. INTRODUCTION

Bismuth tellurohalides belong to layered polar semiconductors lacking the inversion symmetry. One of these semiconductors, BiTeI, has long been a subject of intensive theoretical and experimental investigations[1–8] focused on electrical, optical, and thermodynamical properties. Detailed information on the electronic structure of bismuth tellurohalides is now available.[6–9] Much attention has been recently paid to these compounds due to a strong spin-orbit interaction of electrons caused by Bi atoms. When the inversion symmetry is lost, the spin-orbit coupling (SOC) removes spin degeneracy, thereby leading to various novel phenomena such as spin galvanic and Hall effects.[10–13] Another SOC-induced phenomenon in the absence of the inversion symmetry is the Rashba interaction, which has been experimentally demonstrated for BiTeI.[7] The angle-resolved photoemission spectroscopy (ARPES) experiments showed a huge Rashba spin splitting (∼0.4 eV) near the conduction band minimum, which is found to be substantially shifted away from the high symmetry point *A* in the Brillouin zone (BZ). The experimental results were found to be in agreement with first-principles calculations both for bulk and surface electronic states.[7–9] In addition, nanoparticles of BiTeI are of both fundamental and technological interest because it is expected that the semiconductor nanoparticles exhibit a variety of new spectroscopic properties.[14]

While the electronic structure of bismuth tellurohalides is now quite well understood, the lattice dynamics of these semiconductors has not been studied yet. Taking into account properly the influence of spin-orbit coupling on the lattice vibrations of bismuth tellurohalides makes such calculations rather challenging. Scalar relativistic calculations might be less accurate for systems whose electronic structure is considerably modified by spin-orbit coupling.[7–9] In addition, it was shown that for heavy elements, the SOC effects become as important for structural and dynamical properties as for electronic properties.[15,16]

In this paper, we present a theoretical study of the structural and dynamical properties of two bismuth tellurohalides, BiTeI and BiTeCl, by first-principles calculations based on density-functional theory and a detailed comparison with Raman spectroscopy measurements. We also present the experimental Raman spectrum of BiTeBr, which crystallizes in a hexagonal system with statistically distributed Te and Br atoms.[17] Since the effect of spin-orbit interaction on lattice vibrations is of much interest, the calculations were performed in two versions: (i) only scalar relativistic (SR) effects are taken into account, (ii) both SR and spin-orbit effects are included. We also calculate and analyze the transverse-optical longitudinal-optical (LO-TO) splitting of zone-center optical modes. The theoretical frequencies for Raman active modes in BiTeI and BiTeCl are compared to the experimental data from Raman spectra.

The paper is organized as follows. Section II describes the experimental procedure. Section III contains a short outline of the calculation method and the analysis of structural and vibrational properties. Then we focus on the zone-center phonons. The details of the measured Raman spectra for bismuth tellurohalides are given in Sec. IV. Finally, we summarize in Sec. V.

II. EXPERIMENTAL CONDITIONS

In this work synthesis of the charges was performed by fusing binary compounds: Bi_2Te_3 with $BiCl_3$, BiI_3 and $BiBr_3$, correspondingly. According to the published data[1,18] BiTeI and BiTeBr melt congruently at 560° C and 526° C, while BiTeCl

has incongruent melting[18] at 430° C with peritectic composition around 11 mol. % Bi_2Te_3 + 89 mol. % $BiCl_3$. Therefore we have used stoichiometric charge for BiTeI, BiTeBr and melt-solution system with molar ratio $Bi_2Te_3 : BiCl_3 = 1 : 9$ for crystallization of BiTeCl. The synthesis was performed directly in the growth quartz ampoules at 20° C higher than melting point. Thereby the influence of atmospheric water and oxygen was minimized. Crystal growth was done by modified Bridgman method with rotating heat field.[19] After pulling the ampoules through the vertical temperature gradient 15° C/cm with a rate 10 mm/day the furnace was switched off.

For Raman scattering experiments, the 514.5 nm line of an Ar+ laser was used for excitation. Raman spectra were obtained in a Jobin Yvon T64000 spectrometer in the 10 to 1000 cm^{-1} Raman shift range and spectral resolution ~1.5 cm^{-1}. In all cases, Raman spectra were recorded at room temperature, in a backscattering geometry with polarized incident light and with analyzer of scattered light. "Parallel" polarization geometry (the polarization of scattered light was parallel to the polarization of incident light, VV) and "perpendicular" polarization geometry (the polarization of scattered light was perpendicular to polarization of incident light, UV) were used. All spectra were recorded at low power levels $P <$ 3 mW with the spot size ~50 μm to avoid local laser heating.

III. CALCULATION RESULTS

A. Calculation details

Dynamical properties of BiTeI and BiTeCl were calculated within density-functional perturbation theory[20,21] in a mixed-basis pseudopotential approach.[22–24] The calculations, both scalar relativistic and including spin-orbit coupling, were performed with relativistic norm-conserving pseudopotentials, which were constructed from all-electron valence states according to the scheme given by Vanderbilt.[25] We used the following atomic configurations for the valence space: Bi ($6s^2 6p^{2.75} 6d^{0.25}$), Te ($5s^2 5p^{3.5} 5d^{0.5}$), I ($5s^2 5p^{4.5} 5d^{0.5}$), and Cl ($3s^2 3p^4 3d^0 4s^1$). In all cases, nonlinear core corrections were taken into account. The exchange and correlation energy functional was evaluated within the generalized gradient approximation proposed by Perdew, Burke, and Ernzerhof (GGA-PBE).[26] Further details of the spin-orbit coupling implementation within the mixed-basis pseudopotential method can be found in Ref. 16. The mixed-basis scheme employs a combination of local functions and plane waves to represent valence states.[22,23] The size of the plane wave basis set was restricted to a kinetic energy cutoff of 18 Ry and 24 Ry for BiTeI and BiTeCl, respectively. Additionally, local functions of s, p, and d type at each atomic site were used. Brillouin zone integrations were performed by sampling a 12×12×8 (12×12×4) **k**-point mesh corresponding to 1152 (576) special points in the BZ of BiTeI (BiTeCl).

B. Structural parameters

Since dynamical properties are closely related to the crystal structure of a compound, we first present information on the atomic structure of bismuth tellurohalides. The crystal structure of the compounds was defined from x-ray powder diffraction (XRD) data and then described using a semi-ionic model.[17] It was established that at low temperature the crystal structure of the bismuth tellurohalides is hexagonal. It is presented in Fig. 1 for all three compounds. A characteristic feature of the crystals is the lack of inversion symmetry. The experimental and optimized theoretical hexagonal lattice parameters a and c/a for BiTeI and BiTeCl are given in Table I.

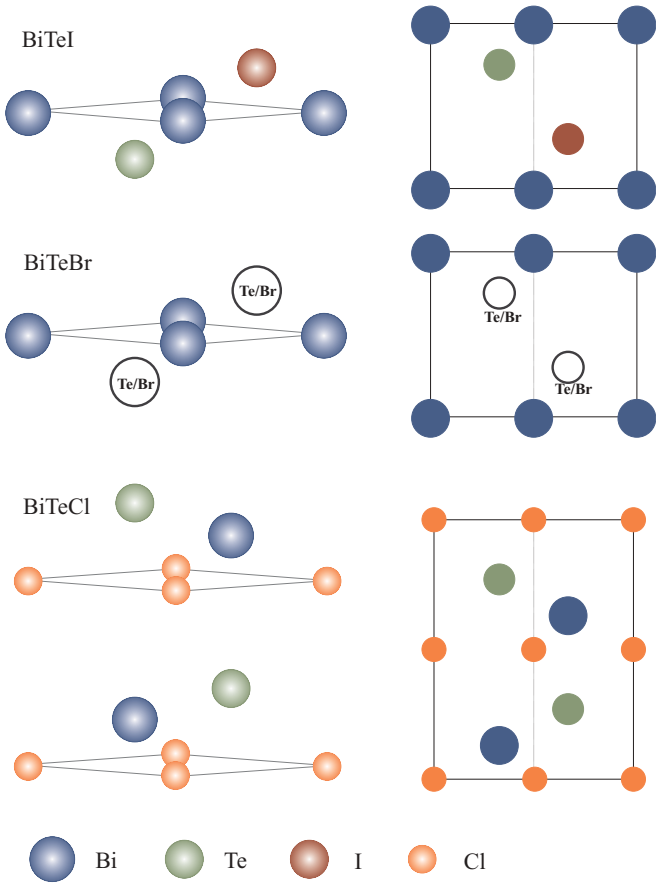

FIG. 1. (Color online) A triple layer of Te-Bi-I and two triple layers of Cl-Bi-Te, forming the unit cell of BiTeI and BiTeCl, respectively. In the middle part, the structure of Te/Br-Bi-Te/Br is shown. Projections of the crystal structures on the $(11\bar{2}0)$ plane are displayed on the right panel.

TABLE I. Structural parameters, bulk moduli B, and pressure derivatives of the bulk moduli dB/dP for BiTeI and BiTeCl. Experimental values are taken from Ref. 17. SOC indicates the calculation including spin-orbit coupling while SR denotes the scalar relativistic one.

	a (a.u.)	c/a	B (MBar)	dB/dP
BiTeI				
SR	8.344	1.566	0.37	4.41
SOC	8.382	1.595	0.33	4.47
Expt.	8.200	1.580		
BiTeCl				
SR	8.119	2.936	0.43	4.45
SOC	8.166	2.982	0.39	3.66
Expt.	8.017	2.922		

The BiTeI crystals consist of a sequence of triple Te-Bi-I layers along the crystallographic hexagonal c axis with three atoms per unit cell. The chemical bonding inside each triple layer is determined by a strong covalency of Bi-Te bonds and ionicity of the Bi-I coupling whereas the triple layers are weakly coupled to each other.[17] In the crystals of BiTeCl, the unit cell contains two triple layers of Cl-Bi-Te rotated relative to each other. The c/a parameter of BiTeCl was found to be nearly twice as large as that of BiTeI whereas the in-plane lattice constants of both compounds are similar.

Besides the hexagonal lattice parameters, a and c/a, the structure of both compounds is determined by internal parameters $\{z_i\}$ describing atomic positions along the c axis. To find the static equilibrium structure, first the total energy E was minimized with respect to the internal parameters $\{z_i\}$ and to the ratio c/a for a set of different volumes V. Then the function $E_{\min}(V)$ was fitted to the Murnaghan equation of state to determine the optimum volume. Finally, the internal parameters $\{z_i\}$ and c/a were optimized again. The optimized structural parameters are summarized in Tables I and II together with the calculated values of bulk moduli and pressure derivatives of the bulk moduli. We report the values obtained both without (SR) and with spin-orbit coupling (SOC) and compare them with available experimental information.[17] The calculated lattice parameters (a and c) are larger then the experimental ones by 2–3% in the case of BiTeI and by 2–4% for BiTeCl. This underbinding is larger along the hexagonal axis (the stacking direction) and the c/a ratio is increased by 1% (2%) for BiTeI (BiTeCl) compared to the corresponding experimental value. Such deviations of the lattice constants are typical for GGA-PBE calculations.

Atomic positions are shown in Table II. The internal parameters obtained for BiTeCl are found to be in good agreement with the experimental values. In the case of BiTeI, the optimized Bi-Te distance along the c axis ($\Delta z \sim 0.25c$) is exactly equal to the experimentally defined Bi-I one[17] and the optimized Bi-I distance ($\Delta z \sim 0.3c$) is, respectively, equal to the experimental Bi-Te one. The results are in complete agreement with the data of another first-principles calculation,[8] which employs the GGA-PBE exchange-correlation functional and the augmented plane wave (APW) plus local orbital method as implemented in WIEN2K program. Thus both theoretical works suggest an exchange of Te and I with respect to the structure obtained in the experiment. This may be attributed to the fact that the Te and I atoms have nearly the same ionic radii and atomic charges and, thereby, must produce rather indistinguishable features in XRD patterns.[8] We note that in the bismuth tellurohalides the Bi atoms have an almost regular octahedral coordination of three Te and three halogen atoms. Selected optimized interatomic distances are compared to the available experimental data in Table III. The Bi-Te distances in both compounds are very close to each other and to the Bi-Cl one while the Bi-I distance is ~9% larger than the others. All the bond lengths vary slightly with substituting the experimental lattice parameters for the theoretical equilibrium ones.

For both compounds, the relativistic corrections lead to a small increase (by ~2%) of the lattice constant along the stacking direction and leave almost unchanged the in-plane lattice parameter, which increases by only 0.5%. The SOC has almost no effect on the internal parameters describing atomic positions along the hexagonal axis which differ by less than 1%. Only the bulk moduli decrease by 9–11% due to the relativistic corrections. Thus the introduction of spin-orbit coupling does not modify significantly the structural properties of the bismuth tellurohalides.

TABLE II. Atomic fractional positions $\{z_i\}$ along the c axis. In BiTeI, Bi atoms are assumed to be at origin (0, 0, 0). In BiTeCl, two Cl atoms are at (0, 0, 0) and (0, 0, 0.5). In-plane fractional positions of atoms in the unit cells are given in parentheses. Also given are the experimental values[17] and the data from another first-principles calculation (Ref. 8).

	BiTeI		BiTeCl	
	Te (2/3, 1/3)	I (1/3, 2/3)	Te (2/3, 1/3) (1/3, 2/3)	Bi (1/3, 2/3) (2/3, 1/3)
SR	0.755	0.301	0.271	0.633
SOC	0.758	0.299	0.268	0.632
APW	0.748	0.308		
Expt.	0.693	0.251	0.281	0.639

TABLE III. Selected optimized interatomic distances (in a.u.) are compared with the reported experimental values (Ref. 17).

	BiTeI		BiTeCl	
	Bi-Te	Bi-I	Bi-Te	Bi-Cl
SR	5.784	6.221	5.730	5.656
SOC	5.820	6.279	5.764	5.701
Expt.	5.743	6.183	5.697	5.697

C. Lattice dynamics

1. *Phonon dispersions*

The dynamical matrices for BiTeI (BiTeCl) were computed on a 6×6×4 (6×6×2) **q**-point grid and then a Fourier interpolation scheme was used to obtain phonon frequencies along high-symmetry directions of the BZ. The results of the first-principles calculation with SOC included are displayed in Fig. 2 for both systems. The right panels of the figure give the phonon density of states (DOS). Since the unit cell of BiTeI (BiTeCl) contains 3 (6) atoms, there are 9 (18) modes of vibration in all. In BiTeI, three acoustic phonon branches have a mixed character characterized by the participation of all types of atoms in the lattice motion. In the case of BiTeCl, these low-energy vibrations are mainly associated with displacements of heavy Bi and Te atoms while the contribution of light Cl atoms to the vibrational amplitude is rather small (Fig. 2, right panel). That also holds for the first three optical branches. In addition, the difference in mass results in a small gap between the lower six phonon branches and the higher optical ones. As concerns the optical modes, in the case of BiTeI, one can distinguish two types of vibrations. The first three optical branches are mainly determined by vibrations of iodine atoms whose contribution to the vibrational amplitude varies between 70% and 85%. The next group of vibrations is mostly associated with the motion

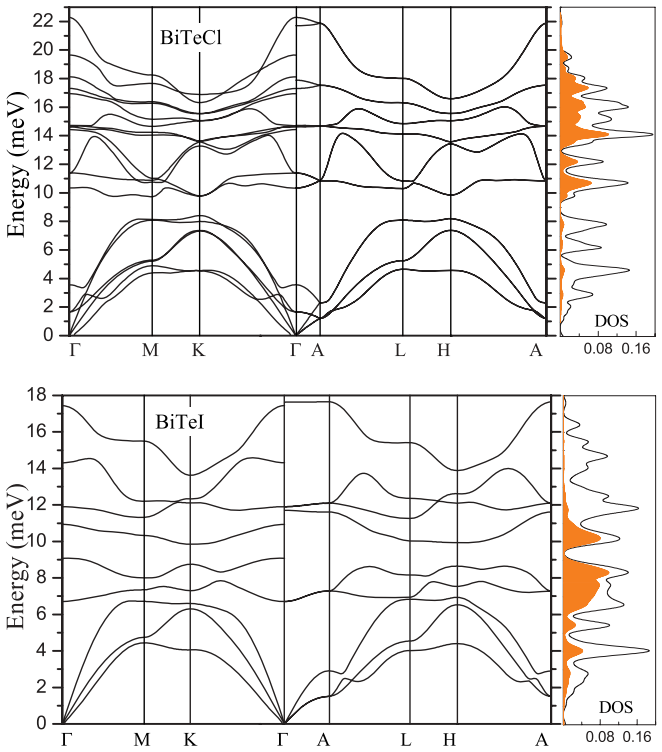

FIG. 2. (Color online) Phonon dispersions of BiTeI and BiTeCl calculated with spin-orbit coupling at the optimized lattice parameters. The right panels show the phonon density of states (DOS). The coloured areas give the partial DOS of halogen atoms.

of Te atoms and, at higher frequencies (>14.5 meV), with the combined vibration of Te and Bi. In the case of BiTeCl, all optical modes except for three low-energy phonon branches are related in a varying degree to the motion of light Cl atoms. Consistent with the expectation of weak coupling along the stacking direction, the dispersion in the ΓA is very small for both compounds.

Figure 3 shows the phonon dispersion calculated with spin-orbit coupling (solid lines) and without SOC (dashed lines). The dispersion for BiTeI is displayed along several symmetry directions of the BZ while for BiTeCl only one symmetry direction, Γ*A*, is shown to demonstrate the principal trend in the behavior of phonon modes when the spin-orbit interaction is added. The calculated phonon frequencies of BiTeI at the A and M symmetry point are also reported in Table IV. In general, for both compounds, the inclusion of spin-orbit interaction causes a shift of the phonon spectrum toward lower frequencies. The difference between the relativistic and scalar relativistic results varies between 0.1–1.2 meV in the case of BiTeI and reaches 2.8 meV for some phonon modes in BiTeCl. The sizable SOC-induced softening of the phonon spectra can be also observed in Fig. 3. However, the softening is already the result of the bigger lattice constants compared to the SR calculation. To separate the effect of the SOC-induced lattice underbinding we have also carried out a SOC calculation with the lattice constants taken from the scalar relativistic case. The obtained phonon frequencies are presented in Table IV. The theoretical evaluation showed that the softening of phonon frequencies due to the SOC-induced lattice underbinding is a main factor for some modes especially those related to the motion of halogen atoms.

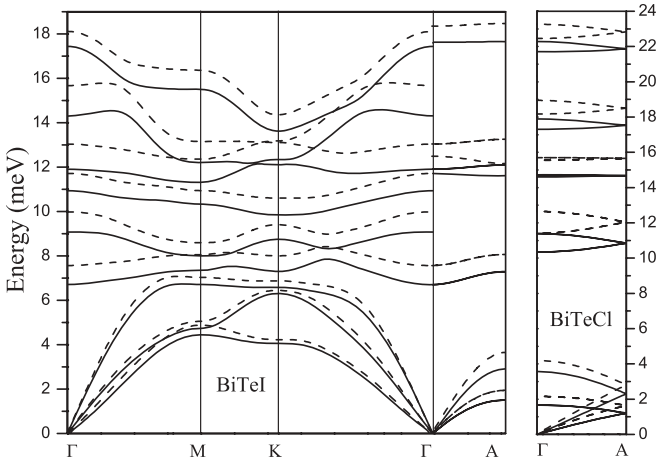

FIG. 3. Phonon dispersions of BiTeI (along some high-symmetry directions of the BZ) and BiTeCl (in the ΓA symmetry line) calculated with (solid lines) and without (dashed lines) spin-orbit coupling included.

TABLE IV. BiTeI: phonon frequencies (in meV) at symmetry points A and M calculated without SOC and including spin-orbit coupling. Δ_{SOC} shows the vibrational frequencies obtained in the calculation including SOC with the lattice parameters taken from the scalar relativistic case. In the first column, the atoms whose contribution to the vibrational amplitude is dominant are indicated. $T_\perp$ and L denote transverse and longitudinal polarizations in the hexagonal plane, respectively, while $T_\parallel$ indicates the polarization along the crystallographic hexagonal axis.

BiTeI	Without SOC	Δ_{SOC}	With SOC
	A		
Bi, Te, I ($LT_\perp$)	1.94	1.83	1.50
Bi, Te, I ($T_\parallel$)	3.65	3.53	2.90
I ($LT_\perp$)	8.06	8.00	7.28
I,Te ($T_\parallel$)	12.16	12.03	11.62
Te ($LT_\perp$)	13.25	12.64	12.10
Te, Bi ($T_\parallel$)	18.47	18.11	17.66
	M		
Bi ($T_\parallel$), Te, I (L)	4.88	4.51	4.45
Bi, Te, I ($T_\perp$)	5.06	4.75	4.74
Bi (L), Te, I ($T_\parallel$)	7.04	6.76	6.71
I ($T_\perp$)	8.06	8.04	7.35
I (L)	8.59	8.58	8.01
I, Te ($T_\parallel$)	10.94	10.80	10.33
Te ($T_\perp$)	12.36	11.88	11.32
Te (L)	13.15	12.73	12.20
Te, Bi ($T_\parallel$)	16.37	16.03	15.50

2. *Zone-center optical phonons*

A complete characterization of the lattice dynamics in the bismuth tellurohalides requires knowledge of the non-analytic contribution to the dynamical matrix in the long-wavelength limit to estimate the LO-TO splitting of zone center optical modes. All the information required to deal with the nonanalytic part is provided by the macroscopic

TABLE V. Theoretical values of the screened Born-effective charge tensors (independent elements) $Z^*/\sqrt{\epsilon_\perp^\infty}$ obtained in the calculation including SOC.

	BiTeI			BiTeCl	
	$Z_\perp^*$	$Z_\parallel^*$		$Z_\perp^*$	$Z_\parallel^*$
Bi	1.99	0.53	Bi	2.11	0.64
Te	−1.05	0.03	Te	−0.89	0.07
I	−0.95	−0.56	Cl	−1.22	−0.71

dielectric tensor $\epsilon_{\alpha\beta}^\infty$ and Born-effective charges $Z_{\alpha\beta}^*(i)$ for each atom i.[24,27] A perturbative approach to calculating these quantities has not been implemented yet for the mixed-basis scheme. We therefore used the alternative way of extracting the nonanalytic part from calculations for q points in the vicinity of the BZ center along four different directions in the reciprocal space. By this procedure, all matrix elements of the dielectric and Born-effective-charge tensors can be determined except for a single scale factor because only ratios $Z^*/\sqrt{\epsilon^\infty}$ enter the expression for the dynamical matrix. Due to the hexagonal symmetry, the different tensors are diagonal with two independent components labeled in the following as $\perp$ and $\parallel$ (i.e., the component perpendicular and parallel to the hexagonal axis, respectively).

In the calculation including SOC, for both compounds we find a large anisotropy in the dielectric tensor: $\epsilon_\perp/\epsilon_\parallel = 2.17$ and $\epsilon_\perp/\epsilon_\parallel = 2.38$ for BiTeI and BiTeCl, respectively. Unfortunately, there are no available experimental or theoretical data on the dielectric properties of bismuth tellurohalides for comparison. The only information reported so far is the $\epsilon_\perp$ component of the dielectric tensor for BiTeI.[4,5] Independent elements of the Born-effective-charge tensors are given in Table V. For both compounds, the calculated charge tensors are very anisotropic. Such a strong anisotropy with rather small values of $Z_\parallel^*$ compared to the $Z_\perp^*$ indicates that the charge transfer along and perpendicular to the hexagonal axis is significantly different. The largest anisotropy is observed for Te atoms while the charge tensors for halogen atoms with $Z_\perp^*/Z_\parallel^* = 1.7$ are much less anisotropic. A large part of the anisotropy is caused by the spin-orbit coupling of electrons. Without spin-orbit interaction we find the anisotropy of dielectric tensor being 30–40% smaller than it was in the SOC calculation. Similarly, the anisotropy of effective charge tensor for Bi atoms decreases by 20%. However, the ratio $Z_\perp^*/Z_\parallel^*$ for halogen atoms is affected weakly.

Tables VI and VII report the calculated zone-center phonon frequencies. In the case of BiTeI, two optical modes belong to A_1 and two to the twofold degenerate symmetry class E. All optical phonons are infrared (IR) and Raman active at the same time. We note that the Raman and IR active modes are not mutually exclusive because of lack of inversion symmetry in the crystal. For BiTeCl, we obtained five E type optical phonons. Two of them and two A_1 modes are both infrared and Raman active, whereas the remaining three E modes are only Raman active, and three A_1 modes are silent. In Sec. IV, the calculated frequencies of the Raman active modes are compared to the experimental data. Here the infrared active modes which exhibit LO-TO splitting at the BZ center are of interest to us. The splitting is found to be significant in both compounds. The largest splitting is observed for lattice vibrations polarized within the hexagonal plane (E). Its value is equal to ∼3 meV in BiTeI and reaches more than 4 meV in the case of BiTeCl. For lattice vibrations polarized along the stacking axis the splitting is significantly smaller, 1–2 meV, and even does not exceed 0.2 meV for the highest energy mode in BiTeI. The large LO-TO splitting of in-plane polarized modes is due to the large $Z_\perp^*$ effective charges compared to the out of plane components of the tensor (Table V).

TABLE VI. Zone-center optical phonon frequencies (ω) for BiTeI in meV (cm^{-1}). The data are obtained in the calculation including SOC. Since all optical modes are IR and Raman active, both TO and LO frequencies are given.

E		A_1	
ω_{TO}	ω_{LO}	ω_{TO}	ω_{LO}
6.71 (54)	9.07 (73)	10.93 (88)	11.71 (94)
11.91 (96)	14.31 (115)	17.44 (141)	17.63 (142)

TABLE VII. Zone-center optical phonon frequencies in meV (cm^{-1}) obtained for BiTeCl in the SOC calculation. For the IR active modes, both TO and LO frequencies are given.

IR/R	ω_{TO}	ω_{LO}	Raman	
E	10.34 (83)	14.43 (116)	E	1.67 (13)
	14.72 (119)	18.12 (146)		11.39 (92)
				14.63 (118)
			silent	
A_1	16.94 (137)	17.89 (144)	A_1	3.56 (29)
	19.65 (158)	21.71 (175)		17.31 (140)
				22.28 (180)

IV. RAMAN SPECTRA OF BISMUTH TELLUROHALIDES

Experimental Raman spectra for all three bismuth tellurohalides are presented in Fig. 4. The geometry with the polarization of scattered light parallel (VV, black solid line) and perpendicular (UV, red dotted line) to the polarization of the incident light is used. The spectra were recorded at room temperature and at low power levels to avoid local laser heating. The Raman spectra of BiTeI and BiTeBr are rather alike. For both compounds, three dominant peaks are observed. For BiTeI, we can make an analysis of the experimental data using information on the Raman active modes obtained theoretically. Since we did not calculate the Raman scattering spectra, we do not give here a precise comparison of the experimental and theoretical data. However, we find a close correspondence in frequency between the position of measured Raman peaks (Fig. 4) and predicted Raman active modes shown in Table VI. The difference does not exceed 5.5 cm^{-1} (0.7 meV). We refer mainly to the calculated TO frequencies, ω_{TO}. LO modes are supposed to be not observed, at least E modes. As regarding the LO frequencies of the A_1 modes, they

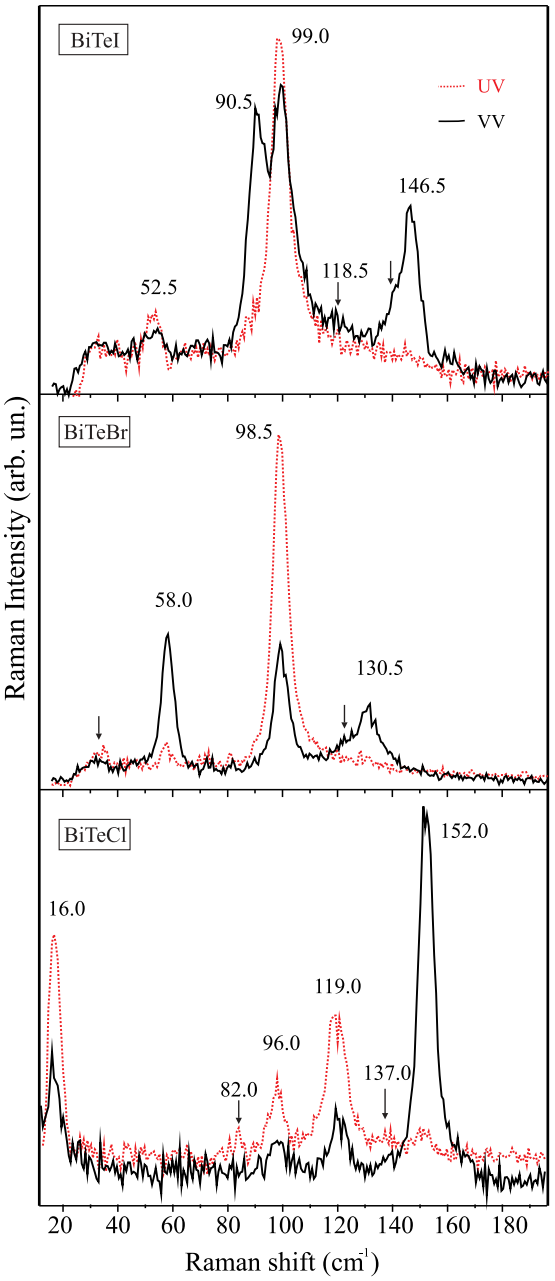

FIG. 4. (Color online) Experimental Raman spectra of BiTeI, BiTeBr, and BiTeCl. The spectra were measured in the geometry when the polarization of scattered light was parallel (VV, black solid line) and perpendicular (UV, red dotted line) to the polarization of the incident light.

are almost side-by-side to the positions of the corresponding TO modes.

In BiTeI, there are four Raman active modes: two degenerate E modes and two A_1 modes. While the E modes can be observed in both scattering geometries (UV and VV), the A_1 modes only appear in the VV spectra. The lowest Raman active mode observed experimentally at 52.5 cm^{-1} and the highest one centered around 146.5 cm^{-1} can be associated with the Raman active modes obtained in the calculation at 54 cm^{-1} (E) and 141 cm^{-1} (A_1), respectively. Both modes are

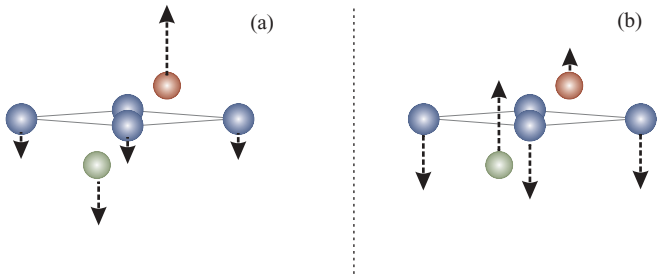

FIG. 5. (Color online) Atomic displacements for two A_1 modes in BiTeI: at (a) 88 cm^{-1} and (b) 141 cm^{-1}.

characterized by the in-phase motion of boundary atoms in the Te-Bi-I trilayer (Te and I) accompanied by displacements of Bi atoms in the opposite direction. For the lowest mode, E, these vibrations are perpendicular to the hexagonal (stacking) axis and are substantially related to the motion of I atoms whose contribution to the vibrational amplitude amounts to 60%. For the highest mode, the sublattices of Bi and Te (I) are vibrating against one another along the stacking direction. Atomic displacements for the A_1 mode are shown schematically in Fig. 5(b). Two Raman active modes obtained in the calculation at 88 cm^{-1} (A_1) and 96 cm^{-1} (E) are mostly determined by the opposite in phase motion of the outer trilayer atoms, Te and I, along and perpendicular to the hexagonal axis, respectively. The modes can be associated with the double Raman peak, centered in the experiment at 90.5 cm^{-1} and 99 cm^{-1}. The A_1 mode (88 cm^{-1}) consists of stretching (Bi-Te)$\Leftrightarrow$ I vibrations shown schematically in Fig. 5(a). For such displacements the force constants along the stacking axis are very important in determining the mode frequency. It applies equally to the A_1 mode obtained in the calculation at 141 cm^{-1} [Fig. 5(b)]. A small feature shown in Fig. 4 at 118.5 cm^{-1} lies close to the calculated position of a longitudinally polarized mode at 115 cm^{-1}. From a similarity between the Raman spectra of BiTeI and BiTeBr, one can speculate that according to the selecting rules the peak observed in BiTeBr at 130.5 cm^{-1} can be assigned to mode A_1 while the Raman mode centered at 98.5 cm^{-1} as well as a small feature observed around 30–35 cm^{-1} can be associated with E-type modes. However, the changes in spectra as compared to the BiTeI cannot be understood only from mass effect. Since Br is lighter than I, higher frequencies would be expected in contrast to the observation.

For BiTeCl, there are seven Raman active modes. Unlike BiTeI, in BiTeCl all Raman active modes with atomic displacements along the hexagonal axis, A_1, are higher in frequency than the lattice vibrations perpendicular to the stacking direction, E. The experimental peak observed around 152 cm^{-1} can be assigned to the highest A_1 mode, at 158 cm^{-1}. This mode, like the highest mode in BiTeI, is mainly determined by in phase vibrations of halogen (Cl) and Te atoms whereas another Raman active A_1 mode (at 137 cm^{-1}) is characterized by displacements of the trilayer boundary atoms opposite in phase. However, in both cases, the atoms in different triple layers of the unit cell move in the same direction.

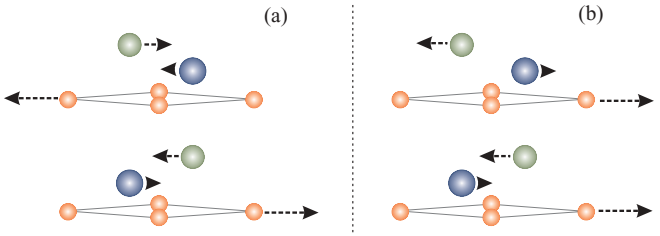

FIG. 6. (Color online) Atomic displacements for two E modes in BiTeCl: at (a) 118 cm^{-1} and (b) 119 cm^{-1}.

Among the E-type Raman active modes one can distinguish two groups. The first one consists of two modes obtained in the calculation at 83 cm^{-1} and 92 cm^{-1}. Both E modes are characterized by in phase vibrations of the boundary atoms, Cl and Te, against the Bi sublattice. In the case of the lower mode, the trilayer boundary atoms of the unit cell move in phase while in the higher one the motion of atoms in different triple layers is opposite to each other. We find that a small peak observed experimentally around 82 cm^{-1} and the next one at 96 cm^{-1} can be assigned to the modes polarized perpendicular to the hexagonal plane and centered at 83 cm^{-1} and 92 cm^{-1}, respectively. The second group consists of two Raman active modes which are very close in frequency (118–119 cm^{-1}) and can be associated with a broad feature observed experimentally around 119 cm^{-1}. The lattice vibrations are determined by displacements of the boundary atoms, Cl and Te, in the opposite directions inside the hexagonal plane. Like the previous case, the motion of atoms in different triple layers of the unit cell is in phase for one mode and is opposite in phase for the other. They are shown schematically in Fig 6. The lowest feature observed experimentally around 16 cm^{-1} can be associated with opposite in-phase displacements of the Te-Bi-Cl trilayers as a whole in the hexagonal plane (the calculated frequency is 13 cm^{-1}).

V. SUMMARY

We presented a study of the structural and dynamical properties of bismuth tellurohalides, BiTeI and BiTeCl, using both first-principles calculations in the density functional perturbation formalism and Raman spectroscopy measurements. It is found that the optimized structural parameters give a small lattice underbinding, which is slightly enhanced when relativistic corrections are added. The underbinding is larger along the hexagonal axis (stacking direction). For both compounds, we find the dielectric and Born-effective-charge tensors very anisotropic, which is appreciably caused by the spin-orbit coupling of electrons. In the scalar relativistic calculation, the anisotropy of dielectric tensor decreases by 30–40% compared to the SOC case. For both compounds, the inclusion of relativistic corrections also leads to a sizable softening of phonon frequencies. However, the softening is partly the effect of the SOC-induced enhancement of lattice underbinding. The latter is a major cause of the softening in the case of modes related to the motion of halogen atoms. In BiTeCl, the difference in mass between Cl and other atoms results in a small gap between the low-frequency phonon branches and the high-frequency optical modes. The zone-center LO-TO splitting is found to be significant in both compounds especially for lattice vibrations polarized within the hexagonal plane due to the large in-plane effective charges compared to the out-of-plane (along the stacking direction) components of effective charge tensors. We also find a close correspondence between the position of measured Raman peaks and the predicted Raman active mode frequencies.

ACKNOWLEDGMENTS

We acknowledge financial support of the University of the Basque Country UPV/EHU (Grant No. GIC07-IT-366-07), the Departamento de Educación del Gobierno Vasco, and the Spanish Ministerio de Ciencia e Innovación (Grant No. FIS2010-19609-C02-01).

[1] A. Tomokiyo, T. Ocada, and S. Kawano, JPN J. Appl. Phys. **16**, 291 (1977).
[2] J. Horak, T. Lichy, and P. Lostak, Phys. Status Solidi A **63**, 407 (1981).
[3] M. B. Babanly, J.-C. Tedenac, Z. S. Aliyev, and D. V. Balitsky, J. Alloy. Compd. **481**, 349 (2009).
[4] J. Horak, J. Phys. (Paris) **31**, 121 (1970).
[5] P. Lostak, J. Horak, A. Vasco, and T. D. Nguyen, Phys. Status Solidi A **59**, 311 (1980).
[6] V. N. Kulbachinskii, V. G. Kytin, Z. V. Lavrukhina, A. N. Kuznetsov, and A. V. Shevelkov, Semiconductors **44**, 1548 (2010).
[7] K. Ishizaka, M. S. Bahramy, H. Murakawa, M. Sakano, T. Shimojima, T. Sonobe, K. Koizumi, S. Shin, H. Miyahara, A. Kimura, K. Miyamoto, T. Okuda, H. Namatame, M. Taniguchi, R. Arita, N. Nagaosa, K. Kobayashi, M. Murakami, R. Kumai, Y. Kaneko, Y. Onose, and Y. Tokura, Nature Mater. **10**, 521 (2011).
[8] M. S. Bahramy, R. Arita, and N. Nagaosa, Phys. Rev. B **84**, 041202(R) (2011).
[9] S. V. Eremeev, I. A. Nechaev, Y. M. Koroteev, P. M. Echenique, and E. V. Chulkov, Phys. Rev. Lett. **108**, 246802 (2012).
[10] S. D. Ganichev, E. L. Ivchenko, V. V. Belkov, S. A. Tarasenko, M. Sollinger, D. Weiss, W. Wegscheider, and W. Prettl, Nature (London) **417**, 153 (2002).
[11] V. Sih, R. C. Myers, Y. K. Kato, W. H. Lau, A. C. Gossard, and D. D. Awschalom, Nature Phys. **1**, 31 (2005).
[12] S. Takahashi and S. Maekawa, Sci. Technol. Adv. Mater. **9**, 014105 (2008).
[13] I. M. Miron, G. Gaudin, S. Auffret, B. Rodmacq, A. Schuhl, S. Pizzini, J. Vogel, and P. Gambardella, Nature Mater. **9**, 230 (2010).
[14] C. Wang, K. Tang, Q. Yang, J. Hu, and Y. Qian, J. Mater. Chem. **12**, 2426 (2002).
[15] M. J. Verstraete, M. Torrent, F. Jollet, G. Zérah, and X. Gonze, Phys. Rev. B **78**, 045119 (2008).
[16] R. Heid, K.-P. Bohnen, I. Yu. Sklyadneva, and E. V. Chulkov, Phys. Rev. B **81**, 174527 (2010).

[17]A. V. Shevelkov, E. D. Dikarev, R. V. Shpanchenko, and B. A. Popovkin, J. Solid State Chem. **114**, 379 (1995).
[18]U. Petasch, C. Hennig, and H. Oppermann, Z. Naturforsch. B **54**, 234 (1999).
[19]K. A. Kokh, B. G. Nenashev, A. E. Kokh, G. Yu. Shvedenkov, J. Cryst. Growth **275**, E2129 (2005).
[20]N. E. Zein, Sov. Phys. Solid State **26**, 1825 (1984) [Fiz. Tverd. Tela (Leningrad) **26**, 3028 (1984)].
[21]S. Baroni, S. de Gironcoli, A. Dal Corso, and P. Giannozzi, Rev. Mod. Phys. **73**, 515 (2001).
[22]S. G. Louie, K.-M. Ho, and M. L. Cohen, Phys. Rev. B **19**, 1774 (1979).
[23]B. Meyer, C. Elsässer, F. Lechermann, and M. Fähnle, FORTRAN90, Program for Mixed-Basis-Pseudopotential Calculations for Crystals (Max-Planck-Institut für Metallforschung, Stuttgart).
[24]R. Heid and K.-P. Bohnen, Phys. Rev. B **60**, R3709 (1999).
[25]D. Vanderbilt, Phys. Rev. B **32**, 8412 (1985).
[26]J. P. Perdew, K. Burke, and M. Ernzerhof, Phys. Rev. Lett. **77**, 3865 (1996).
[27]P. Giannozzi, S. de Gironcoli, P. Pavone, and S. Baroni, Phys. Rev. B **43**, 7231 (1991).